Journal of Alloys and Compounds 507 (2010) 279–285

Contents lists available at ScienceDirect

Journal of Alloys and Compounds

journal homepage: www.elsevier.com/locate/jallcom

Characterization of nanometric multidoped ceria powders

M. Stojmenović[a], S. Bošković[a], S. Zec[a,*], B. Babić[a], B. Matović[a], D. Bučevac[a], Z. Dohčević-Mitrović[b], F. Aldinger[c]

[a] Institute of Nuclear Sciences Vinča, Mihajla Petrovića-Alasa 12-14, POB 522, 11001 Belgrade, University of Belgrade, Serbia
[b] Institute of Physics, Pregrevica 118, POB 68, 11080 Belgrade, Serbia
[c] Max-Planck Institute, Heisenbergstrasse 1, 70569 Stuttgart, Germany

ARTICLE INFO

Article history:
Received 27 April 2010
Received in revised form 15 July 2010
Accepted 17 July 2010
Available online 4 August 2010

Keywords:
Nanostructured materials
Oxide materials
Solid solutions
Vacancy formation
X-ray diffraction
TEM

ABSTRACT

The ceria solid solutions doped with rare earth cations were synthesized by two methods and the microstructural and morphological characterization of powders was performed. The results obtained by X-ray diffraction (XRD), transmission electron microscopy (TEM), Brunauer–Emmett–Teller (BET) method and Raman spectroscopy were studied and discussed. The results showed that finer powders have not only higher specific surface area, smaller particles and crystallite sizes, but also larger lattice parameters in the case of both single and multidoped solid solutions.

1. Introduction

Expected properties of SOFC-s (solid oxide fuel cell) such as high efficiency, low working temperatures, expected low cost of production without environmental pollution, make materials based on cerium oxide of great interest. Due to high ionic conductivity, nanometric powders of cerium oxide (CeO_2) with fluorite structure and especially those doped with rare earth ions became very interesting for research and application as ceramic electrolytes [1–4]. Since the conductivity of nanocrystalline materials increases with decreasing grain size [5], nanocrystalline powders are preferred in the fuel cells production because they enable considerable lowering of sintering temperature leading finally to smaller grain size and lower energy consumption. In addition, the published results on the electrical conductivity measurements proved that the values in the case of multidoped material compared to single doped were 30% higher [6].

With this intention, we made the ultrafine CeO_2 powders doped with many rare earth ions (Nd, Sm, Gd, Dy, Y, Yb) expected them to have high ionic conductivity on lower temperatures due to the formation of oxygen vacancies and microstructural changes. The vacancies are formed in CeO_2 solid solutions by substitution of tetravalent cerium ions with trivalent rare earth ions [7]. In our previous papers [8,9] we were predominantly dealing with single doped ceria solid solutions obtained by two different methods. In this paper however, using the same methods, ceria solid solutions multidoped with rare earth cations were produced and the properties of powders with the same chemical compositions, but obtained by different chemical methods, were studied and discussed.

2. Experimental

Experimental work consisted of the synthesis and characterization of nanopowders with the following composition:

1. CeO_2, 2. $Ce_{0.8}Gd_{0.20}O_{2-\delta}$, 3. $Ce_{0.8}Sm_{0.08}Gd_{0.12}O_{2-\delta}$, 4. $Ce_{0.8}Sm_{0.01}Gd_{0.01}Y_{0.18}O_{2-\delta}$, 5. $Ce_{0.8}Sm_{0.005}Gd_{0.005}Dy_{0.095}Y_{0.095}O_{2-\delta}$, 6. $Ce_{0.8}Nd_{0.01}Sm_{0.04}Gd_{0.04}Dy_{0.04}Y_{0.07}O_{2-\delta}$, 7. $Ce_{0.8}Nd_{0.01}Sm_{0.015}Gd_{0.025}Dy_{0.04}Y_{0.05}Yb_{0.06}O_{2-\delta}$, Nanopowders were synthesized using modified glycine nitrate procedure (MGNP) [8] and self-propagating reaction at room temperature (SPRT) [9].

2.1. Synthesis by MGNP method

Nanometric powders of cerium oxide solid solutions were obtained by MGNP method, starting from amino acetic acid (glycine, Fluka) and solutions of nitrate of following ions Ce, Nd, Sm, Gd, Dy, Y (Aldrich). The syntheses of doped nanopowders proceeded according to the following exothermic reaction:

$$4NH_2CH_2COOH + 2[(1-x)Ce(NO_3)_3{\cdot}6H_2O + xMe(NO_3)_3{\cdot}6H_2O] + 2O_2 \rightarrow 2Ce_{1-x}Me_xO_{2-\delta} + 22H_2O\uparrow + 5N_2\uparrow + 8CO_2\uparrow \quad (1)$$

Modification consisted of partial substitution of nitrates by acetates [8]. Rare earth ions (dopants) were used in total concentration of $x = 0.2$. Syntheses were carried

* Corresponding author. Tel.: +381 11 3408673; fax: +381 11 3408224.
E-mail address: zec@vinca.rs (S. Zec).

0925-8388/$ – see front matter © 2010 Elsevier B.V. All rights reserved.
doi:10.1016/j.jallcom.2010.07.177

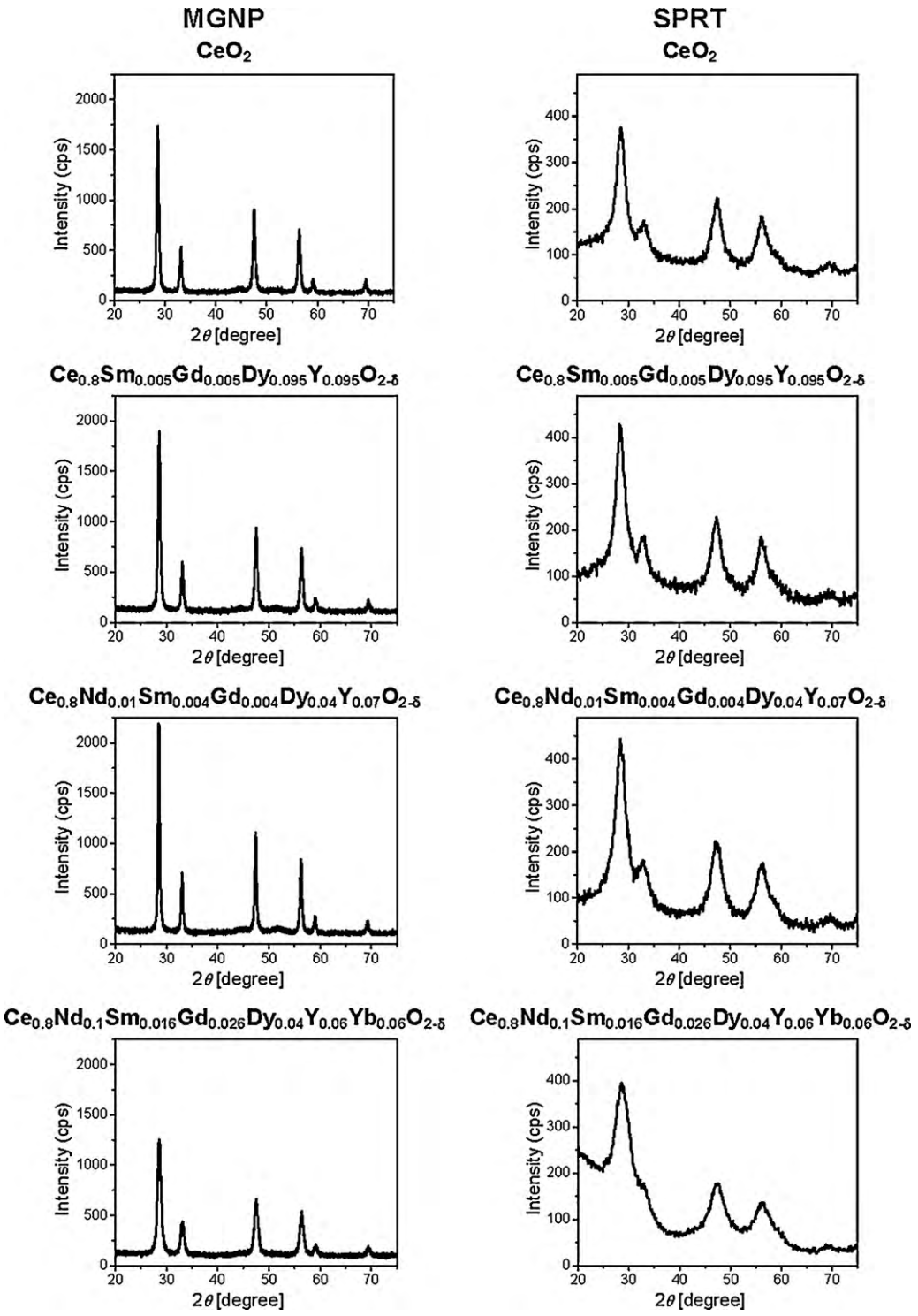

Fig. 1. XRD patterns of nanopowders obtained by MGNP and SPRT methods.

out in a steel beaker. All the reactants dissolved in distilled water were added in concentrations previously calculated according to the relation (1). Reacting mixtures were heated up to 450 °C until the evaporation stopped. Due to the modification, moderate reaction has occurred, and dissipation of the ash during synthesis was very small. In the end, obtained ash was calcined at 600 °C during 4 h to burn up the organic remains.

2.2. Synthesis by SPRT method

SPRT method was used to obtain solid solutions with the same composition as nanopowders prepared by MGNP method. SPRT method is based on the mechanically activated reaction between metal nitrates (cerium and dopants) and sodium hydroxide, which occurred at room temperature according to the Eq. (2):

$$2[(1-x)Ce(NO_3)_3{\cdot}6H_2O + xMe(NO_3)_3{\cdot}6H_2O] + 6NaOH + (1/2-\delta)O_2 \rightarrow 2Ce_{1-x}Me_xO_{2-\delta} + 6NaNO_3 + 15H_2O \quad (2)$$

The advantage of this method is the possibility of producing the nanopowders without heating and additional calcinations. Basic reactants for synthesis were nitrates of following ions Ce, Nd, Sm, Gd, Dy, Y (Aldrich) and NaOH (Vetprom – Chemicals). Quantities of reactants needed for SPRT syntheses were calculated by the Eq. (2).

Syntheses of pure and doped CeO_2 nanopowders was carried out according to the procedure described in detail in Refs. [8,9].

2.3. Powder characterization

With the aim of comparing properties of powders synthesized by described methods, they were characterized by X-ray diffraction (XRD), transmission electron microscopy (TEM), Brunauer–Emmett–Teller (BET) method and Raman spectroscopy.

XRD analysis was performed by Siemens D-500 diffractometer using CuK_α radiation and scanning speed of $0.02^\circ 2\theta/s$. Lattice parameter, crystallite size and deformation of crystal lattice, i.e. microstrain were calculated from X-ray data collected in the range of $20–75^\circ 2\theta$. Lattice parameter was calculated by WIN-CELL program. Crystallite size and microstrain were determined according to the Williamson–Hall method using Cauchy relation between contributions of crystallite size and lattice distortion to the width of diffraction profile [10]. We have measured width of diffraction profiles in the middle of diffraction peak height. Widths of well-crystallized α-quartz reflections were measured in the same way in order to determine instrumental width, i.e. the part of diffraction profile originated from spectral width of radiation and diffractometer setting. Eliminating instrumental width from diffraction profiles [11], the width originating from crystallite size and lattice distortion was determined.

Specific surface areas of powders were obtained by BET method based on adsorption and desorption isotherms, that represent the amount of N_2 adsorbed at −196 °C as a function of relative pressure and were measured using the gravimetric McBain method. Besides the specific surface area, also the pore size distribution, mesopore surface and micropore volume were calculated from the isotherms. Pore size distribution was obtained by applying BJH method [12] to the desorption branch of isotherms. Mesopore surface and micropore volume were estimated using the high resolution α_s-plot method [13–15]. Micropore surface was calculated by subtracting mesopore surface from specific surface area. Powder flow was performed by applying internal comparative method. The same weights of powders were poured into the funnel and the time in which the powder run out of the funnel was measured for each powder. The following results are obtained: 32 s for MGNP and 1 s for SPRT powders, showing that SPRT powders flew much faster out of the funnel.

Particles size for MGNP powders was measured by TEM – ZEISS EM 912 Omega, while for SPRT it was measured on TEM micrographs using the computer program Digital Micrograph, after the micrographs had been taken by JEOL 400 FX instrument. The differences in particle size were proved to be like previously obtained [16].

Raman spectroscopy was performed in the backscattering configuration using the Jobin Yvon T64000 spectrometer system. The measurements were made at room temperature with the 514.5 nm Ar^+-ion laser line in the spectral range 200–800 cm^{-1}.

3. Results and discussion

Characterization of synthesized nanopowders was done with the intention to establish differences in the powder properties produced by MGNP and SPRT methods, since the powder history has a strong influence on the microstructure and morphology of powder particles.

The X-ray patterns (Fig. 1) show that synthesized powders are single phase, indicating that the dopants are incorporated in ceria lattice instead of Ce^{4+} ions. Besides, the lattice parameters (Table 1) of the identified fluorite structures in the X-ray patterns verified formation of ceria solid solutions according to the previously found results [7,8] by which the parameters of ceria lattice increase according to the Vegard's law with increasing dopants concentration (Gd, Sm, Nd). The values of lattice parameter (a), crystallite size (D) and microstrain (e) obtained by XRD analysis are summarized in Table 1.

For powders with particle size smaller than 5 nm obtained by SPRT method, lattice parameters are larger as compared to MGNP powders with much larger particles, 25–40 nm (Table 3). The results are in accordance with literature data concerning the anomaly of relatively strong increase of ceria lattice parameter with decreasing particle size below 10 nm [17–19]. This anomaly is ascribed to an increased concentration of Ce^{3+}-ions with larger ionic radius [17–19]. Also, crystallite sizes (Table 1) of obtained MGNP powders are several times larger in comparison with the values obtained for SPRT powders. The very width of diffraction profiles (Fig. 1) leads to such conclusion.

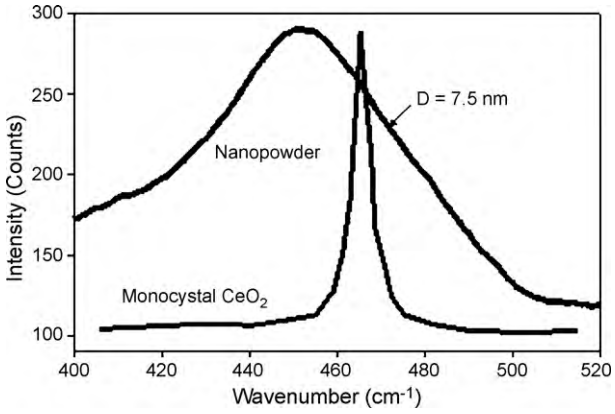

Fig. 2. Dependence of Raman mode position and shape on the particle size of ceria nanopowder [20].

The values of microstrain (Table 1) are significantly higher in nanopowders synthesized by MGNP method, compared to SPRT method. Larger MGNP particles are most likely composed of considerable number of crystallites, which are non-coherently oriented within the particle thus creating higher microstrains upon each other. On the other hand, smaller SPRT particles are composed of just few crystallites because their dimensions are 3–5 nm only. It was also found that large number of dopants did not show any regularity in the change of crystallite size within MGNP powders. However, with the powders obtained by SPRT method it was observed that crystallite size tends to decrease with increased number of dopants (Table 1).

By applying Raman spectroscopy, we found that all the synthesized powders were single phase, which was also found by XRD. The influence of particle size on the position and shape of Raman mode for pure ceria is illustrated in Fig. 2. The results for nanocrystalline ceria show that F_{2g} mode was shifted towards lower frequencies, with decreasing nanoparticle size. The same effect of SPRT and MGNP powders was observed in this study (Fig. 3). With SPRT powders, particle size is considerably lower and the Raman profiles show that F_{2g} mode is shifted to 458 cm^{-1}. On the other hand, MGNP powders with larger particle size show F_{2g} mode position at 465 cm^{-1} indicating well ordered crystalline lattice. In addition, the peaks are narrow due to larger particle size in comparison with SPRT powders, which is in accordance with XRD results.

However, an additional Raman mode of the second order [21] appeared (Fig. 3) with SPRT powder at 600 cm^{-1}. This mode is also related to particle size. Namely, with decreasing particle size in undoped ceria the overall free surface of powder increases enabling easier release of oxygen from the lattice, leaving the vacancy and two electrons localized on cerium atoms. This causes lowering of cerium ion valence due to electroneutrality demands. Additionally, it was found earlier [17] that doped nanopowders show another Raman mode at 545 cm^{-1} which is related to oxygen vacancies formed due to the presence of dopant ions. All these effects can be seen in Fig. 3.

Nitrogen adsorption isotherms are shown in Fig. 4. According to the IUPAC clasification [22] isotherms of MGNP powders (Fig. 4(a)) belong to type-IV with a hysteresis loop which is assosiated with mesoporous materials. Pore size distribution (PSD) for pure and dopped ceria samples obtained by MGNP method is shown in Fig. 4(a) (inset). The distribution for all the samples shows that samples are mesoporous while the amount of micropores is negligible. Similarly, according to the IUPAC clasification isotherms obtained for SPRT powders (Fig. 4(b)) are also of type-IV with a hysteresis loop. Pore size distribution (PSD) for these powders is shown in Fig. 4(b) (inset). The distribution for these samples shows that

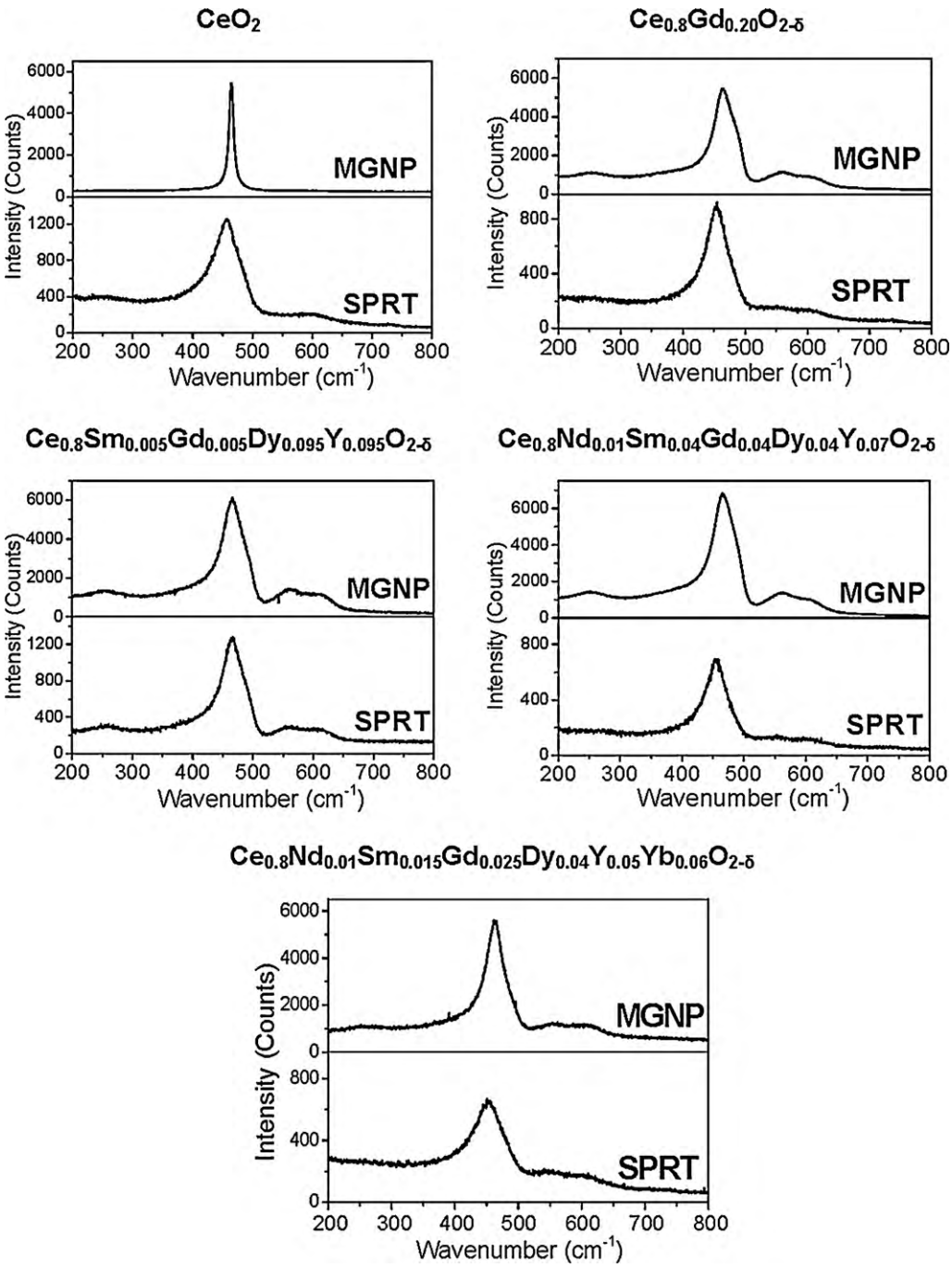

Fig. 3. Raman spectra of nanopowders obtained by MGNP and SPRT methods.

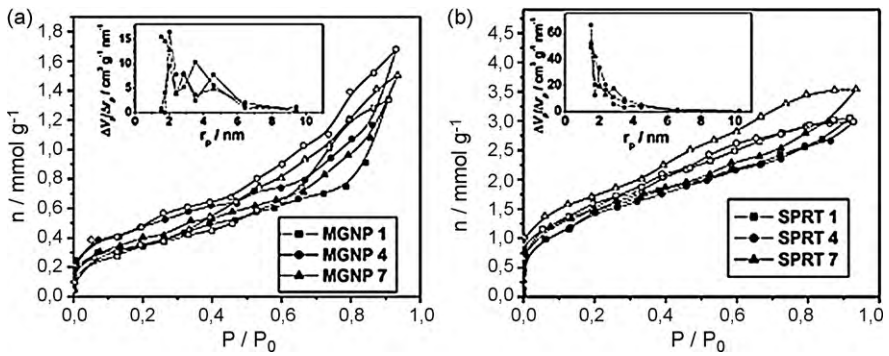

Fig. 4. Nitrogen adsorption isotherms: (a) MGNP and (b) SPRT powders. Solid symbols – adsorption, open symbols – desorption. Inset – pore size distribution (PSD).

Table 1
Lattice parameter (a), crystallite size (D) and microstrain (e) of nanopowders obtained by MGNP and SPRT methods.

Composition	MGNP			SPRT		
	a (Å)	D (nm)	e (%)	a (Å)	D (nm)	e (%)
1. CeO_2	5.4129	16.9	1.18	5.4143	4.3	0.01
2. $Ce_{0.8}Gd_{0.20}O_{2-\delta}$	5.4163	22.5	0.81	5.4284	4.0	0.46
3. $Ce_{0.8}Sm_{0.08}Gd_{0.12}O_{2-\delta}$	5.4322	10.2	2.89	5.4284	5.4	0.69
4. $Ce_{0.8}Sm_{0.01}Gd_{0.01}Y_{0.18}O_{2-\delta}$	5.4118	11.0	2.54	5.4109	3.3	0.75
5. $Ce_{0.8}Sm_{0.005}Gd_{0.005}Dy_{0.095}Y_{0.095}O_{2-\delta}$	5.4141	15.5	1.56	5.4266	3.8	0.06
6. $Ce_{0.8}Nd_{0.01}Sm_{0.04}Gd_{0.04}Dy_{0.04}Y_{0.07}O_{2-\delta}$	5.4248	17.9	0.58	5.4246	3.6	0.33
7. $Ce_{0.8}Nd_{0.01}Sm_{0.015}Gd_{0.025}Dy_{0.04}Y_{0.05}Yb_{0.06}O_{2-\delta}$	5.4137	10.1	3.41	5.4124	2.5	0.31

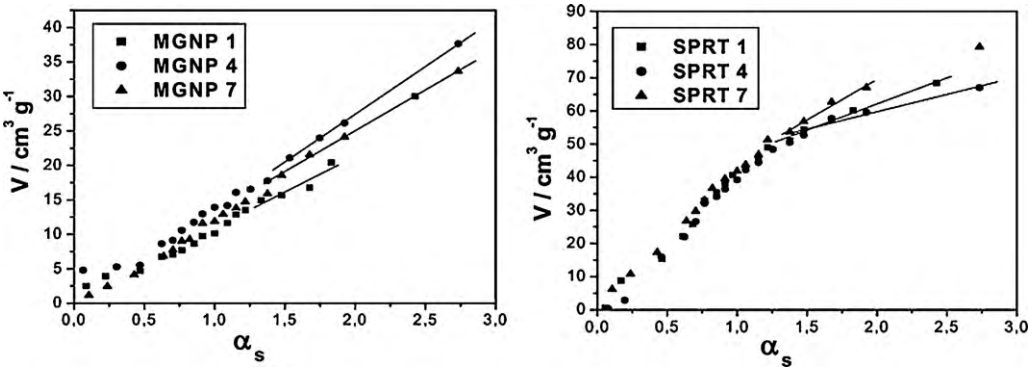

Fig. 5. α_S-Plots for nitrogen adsorption isotherm for MGNP and SPRT powders.

the powders are dominantly microporous with a certain amount of mesoporosity. In both of these cases, adsorption isotherms and PSD for samples which are not presented in Fig. 4(a) and (b) have very similar shape.

Specific surface areas (S_{BET}) calculated by BET equation, are listed in Table 2. All the specific surface values of MGNP powders lie between 13 and 38 m^2/g, while these values for SPRT powders are between 102 and 126 m^2/g. The results do not show any regularity in the change of specific surface area and porosity depending on the number of doping elements for the compositions under study.

Based on the standard nitrogen adsorption isotherms, which are shown in Fig. 4, α_s-plots are obtained (Fig. 5). The slope of straight line in the medium α_s region gives a mesoporous surface area (S_{meso}) including the contribution of external surface, while micropore volume (V_{mic}) is determined by its intercept. Subtraction S_{meso} from S_{BET} gave micropore surface (S_{mic}). Calculated porosity parameters (S_{meso}, S_{mic}, V_{mic}) are also listed in Table 2. Parameters from Table 2 clearly show difference between powders obtained by MGNP and SPRT methods. MGNP powders have lower specific surfaces and only mesopores while SPRT powders predominantly possess higher specific surfaces and developed microporosity (Table 2).

From obtained TEM data (Table 3) it can be seen that sizes of particles synthesized by MGNP are nanometric (14–40 nm, Fig. 6) as well as the nanopowders synthesized by SPRT method, but with smaller particle sizes (3–5 nm, Fig. 6).

Table 3
Particle size of multidoped powders obtained by TEM.

Composition	Particle size (nm)	
	SPRT	MGNP
1. CeO_2	4.91	40
2. $Ce_{0.8}Gd_{0.2}O_{2-\delta}$	4.18	25
3. $Ce_{0.8}Sm_{0.08}Gd_{0.12}O_{2-\delta}$	3.64	–
4. $Ce_{0.8}Sm_{0.01}Gd_{0.01}Y_{0.18}O_{2-\delta}$	3.13	19
5. $Ce_{0.8}Dy_{0.005}Gd_{0.005}Dy_{0.095}Y_{0.095}O_{2-\delta}$	3.22	30
6. $Ce_{0.8}Nd_{0.01}Sm_{0.04}Gd_{0.04}Dy_{0.04}Y_{0.07}O_{2-\delta}$	3.17	15
7. $Ce_{0.8}Nd_{0.01}Sm_{0.015}Gd_{0.025}Dy_{0.04}Y_{0.05}Yb_{0.06}O_{2-\delta}$	2.83	14

Results obtained by TEM showed that size of particles decreased in doped powders as compared to pure ceria powders. The data are also in accordance with the results obtained by XRD method confirming smaller crystallite size of SPRT powders. However, this regularity was not observed with the values of specific surface area, although these two values should be related. The reason for this deviation might be generation of different agglomerates depending on the production method. Namely, the SPRT powders are much less agglomerated as compared to MGNP powders, although it is expected that finer SPRT powders will be agglomerated in a significantly higher degree. Agglomeration of MGNP powders was already detected during pouring the powders into pressing die and was

Table 2
Specific surface area (S_{BET}), specific surface of mesopores (S_{mezo}), specific surface and volume of micropores (S_{mic},V_{mic}) for MGNP and SPRT powders.

Sample	MGNP		SPRT			
	S_{BET} (m^2/g)	S_{meso} (m^2/g)	S_{BET} (m^2/g)	S_{meso} (m^2/g)	S_{mic} (m^2/g)	V_{mic} (cm^3/g)
1. CeO_2	27	27	114	43	71	0.047
2. $Ce_{0.8}Gd_{0.20}O_{2-\delta}$	36	36	112	33	79	0.058
3. $Ce_{0.8}Sm_{0.08}Gd_{0.12}O_{2-\delta}$	38	38	115	44	71	0.054
4. $Ce_{0.8}Sm_{0.01}Gd_{0.01}Y_{0.18}O_{2-\delta}$	38	38	110	29	81	0.060
5. $Ce_{0.8}Sm_{0.005}Gd_{0.005}Dy_{0.095}Y_{0.095}O_{2-\delta}$	13	13	126	50	76	0.049
6. $Ce_{0.8}Nd_{0.01}Sm_{0.04}Gd_{0.04}Dy_{0.04}Y_{0.07}O_{2-\delta}$	19	19	102	59	43	0.032
7. $Ce_{0.8}Nd_{0.01}Sm_{0.015}Gd_{0.025}Dy_{0.04}Y_{0.05}Yb_{0.06}O_{2-\delta}$	30	30	117	70	47	0.032

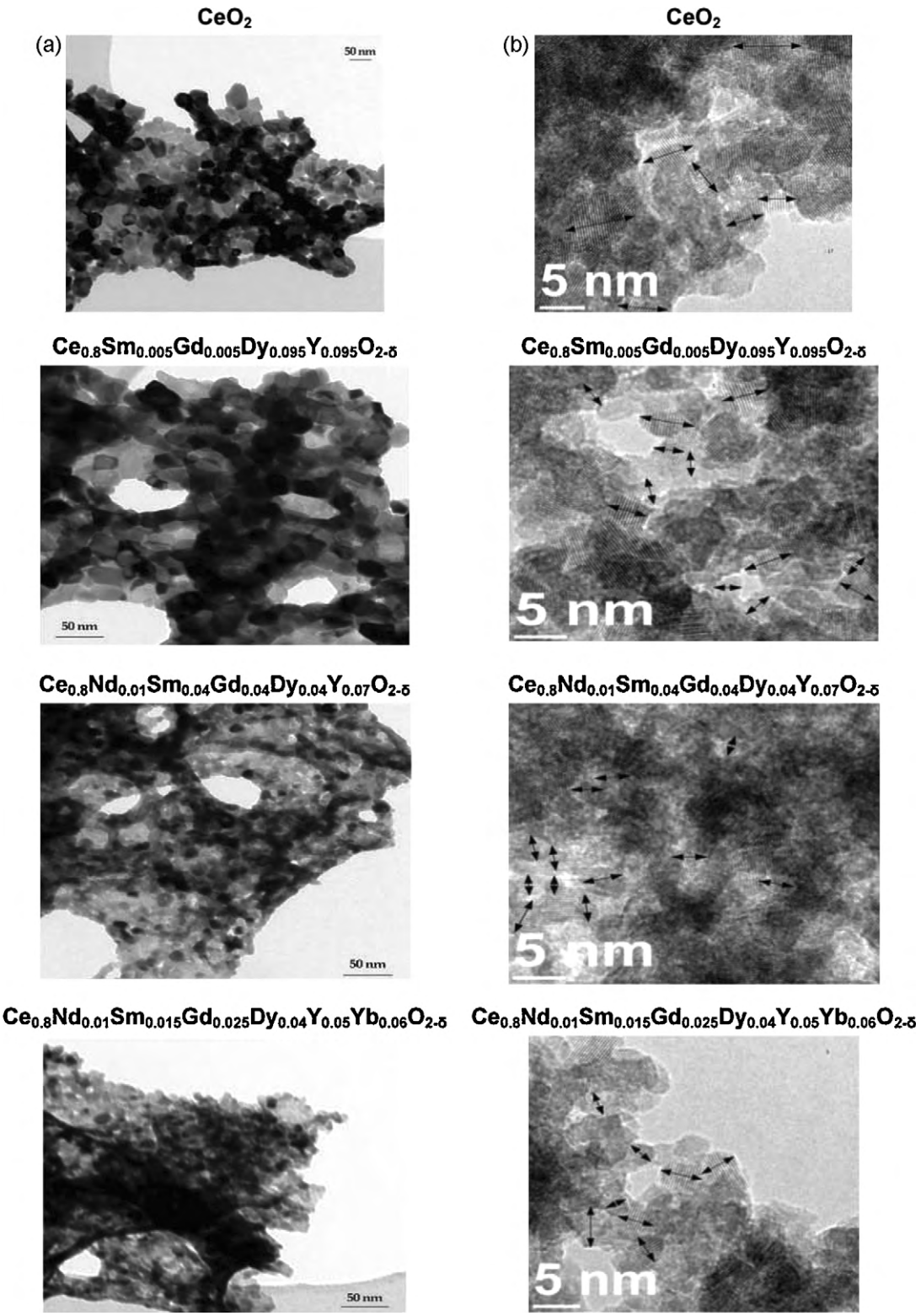

Fig. 6. TEM micrographs: (a) MGNP powders, (b) SPRT powders.

confirmed by measurements of powders flow. We believe that the agglomerates within MGNP powders lower the value of specific surface.

In addition, TEM micrographs show that powders prepared by MGNP method posses large pores within the agglomerates (Fig. 6). This is clearly seen in Fig. 7, $Ce_{0.8}Gd_{0.2}O_{2-\delta}$ composition taken by SEM, which is illustrative for MGNP powders. On the contrary, large pores are not found in TEM micrographs of SPRT powders. Obviously, different types of agglomerations have occurred in the production of nanopowders, which can be related with the effect of the temperature. Heating of reaction mixtures up to 450 °C and the strong exothermic reaction used in MGNP procedure followed by calcinations at 600 °C caused the sintering of ash, which produced hard agglomerates with large pores. On the other hand, the fine

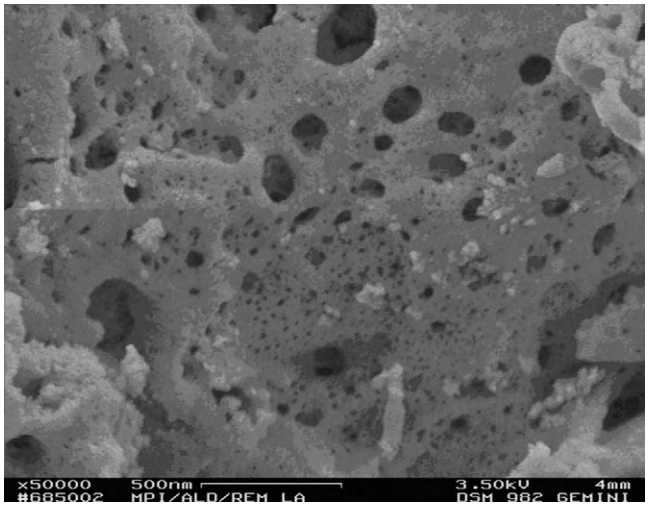

Fig. 7. SEM micrograph of MGNP prepared $Ce_{0.8}Gd_{0.2}O_{2-\delta}$ composition.

SPRT powders do not undergo any thermal treatment and therefore the powders are formed of more soft and microporous aggregates responsible also for the high specific surface area.

Since the question of powders history does not have an answer even not to-day, the differences found so far in the literature [17–19] are usually connected to the particle dimension as measurable parameter. According to the given explanations in this study, we assumed that the different chemical methods and associated thermal effects of MGNP method, opposite to the SPRT-room synthesis, are responsible for differences in the powder properties.

4. Conclusion

After synthesis and characterization of CeO_2 nanopowders produced by both MGNP and SPRT methods as well as comparative analysis of powders, the results may be summarized as follows:

- XRD method and Raman spectroscopy confirmed that all the synthesized nanopowders are single phased
- an additional Raman mode of second order appeared with SPRT powders at 600 cm^{-1}
- there is a difference between values of lattice parameters for samples of the same chemical composition obtained by MGNP and SPRT
- crystallite size differs as well, being larger for MGNP powders
- microstrain values are larger for MGNP powders
- specific surface area is larger with SPRT powders
- difference in type of porosity also exists, i.e. MGNP powders are mesoporous while SPRT powders are predominantly microporous.

Based on these findings, it is obvious that the applied preparation method affects many important properties of the powders under study. Contrary to the expectations, the agglomeration is more pronounced with MGNP powders and the agglomerates are harder due to the thermal effects during the preparation procedure.

Acknowledgements

The authors are grateful to Ministry of Science and Technological Development of the Republic of Serbia and the Humboldt Foundation for supporting the research defined by the project 45012.

References

[1] B.C.H. Steele, Solid State Ionics 134 (2000) 3–20.
[2] B.C.H. Steele, J. Mater. Sci. 36 (2001) 1053–1068.
[3] O. Yamamoto, Electrochim. Acta 45 (2000) 2423–2435.
[4] S.M. Haile, Acta Mater. 51 (2003) 5981–6000.
[5] M. Oljaca, R. Maric, S. Shanmunghan, A. Hunt, Am. Ceram. Soc. Bull. 82 (2003) 38–40.
[6] J. van Herle, D. Seneviratne, A.J. McEvoy, J. Eur. Ceram. Soc. 19 (1999) 837–841.
[7] J.R. McBride, K.C. Hass, B.D. Poindexter, W.H. Weber, J. Appl. Phys. 76 (1994) 2435–2441.
[8] S.B. Bošković, B.Z. Matović, M.D. Vlajić, V.D. Krstić, Ceram. Int. 33 (2007) 89–93.
[9] S. Bošković, D. Đurović, Z. Dohčević-Mitrović, Z. Popović, M. Zinkevich, F. Aldinger, J. Power Sources 145 (2005) 237–242.
[10] B. Lönnberg, J. Mater. Sci. 29 (1994) 3224–3230.
[11] G. Ziegler, Powder Metall. Int. 10 (1978) 70–73.
[12] E.P. Barrett, L.G. Joyner, P.P. Halenda, J. Am. Chem. Soc. 73 (1951) 373–380.
[13] K. Kaneko, C. Ishii, M. Ruike, H. Kuwabara, Carbon 30 (1992) 1075–1088.
[14] M. Kruk, M. Jaroniec, K.P. Gadkaree, J. Colloid Interface Sci. 192 (1997) 250–256.
[15] K. Kaneko, C. Ishii, H. Kanoh, Y. Hanzawa, N. Setoyama, T. Suzuki, Adv. Colloid Interface Sci. 76–77 (1998) 295–320.
[16] S. Boskovic, S. Zec, M. Ninic, J. Dukic, B. Matovic, D. Djurovic, F. Aldinger, J. Optoelectron. Adv. Mater. 10 (2008) 515–519.
[17] S. Tsunekawa, J.-T. Wang, Y. Kawazoe, J. Alloy. Compd. 408–412 (2006) 1145–1148.
[18] S. Tsunekawa, K. Ishikawa, Z.-Q. Li, Y. Kawazoe, A. Kasuya, Phys. Rev. Lett. 85 (2000) 3440–3443.
[19] F. Zhang, S.-W. Chan, J.E. Spanier, E. Apak, Q. Jin, Appl. Phys. Lett. 80 (2002) 127–129.
[20] Z.D. Dohčević-Mitrović, M.J. Šćepanović, M.U. Grujić-Brojčin, Z.V. Popović, B.Z. Matović, S.B. Bošković, Appl. Phys. Lett. 91 (2007) 203118–203120.
[21] W.H. Weber, K.C. Hass, J.R. Mcbride, Phys. Rev. B 48 (1993) 178–185.
[22] K.S.W. Sing, D.H. Everett, R.A.W. Haul, L. Moscou, R.A. Pierotti, J. Rouquerol, T. Siemieniewska, Pure Appl. Chem. 57 (1985) 603–619.